APPLIED PHYSICS LETTERS **101**, 242107 (2012)

Quantitative self-calibrating lock-in carrierographic lifetime imaging of silicon wafers

Qiming Sun,[1,2] Alexander Melnikov,[1] and Andreas Mandelis[1]
[1]*Center for Advanced Diffusion-Wave Technologies (CADIFT), Mechanical and Industrial Engineering, University of Toronto, Toronto M5S 3G8, Canada*
[2]*School of Optoelectronic Information, University of Electronic Science and Technology of China (UESTC), Chengdu 610054, China*

(Received 29 October 2012; accepted 30 November 2012; published online 12 December 2012)

Quantitative self-calibrating lock-in carrierography (LIC) imaging of crystalline silicon wafers is introduced using an InGaAs camera and a spread super-bandgap illumination laser beam. Images at several modulation frequencies and a simplified model based on photocarrier radiometric theory are used to construct the *effective* carrier lifetime image from the phase-frequency dependence. The phase image data at several frequencies and at selected locations on a wafer were compared to frequency scans obtained with a single-element InGaAs detector, and good agreement was found. The quantitative LIC lifetime imaging capability demonstrated in this work is self-calibrating and eliminates the requirement for calibration in conventional photoluminescence imaging. © *2012 American Institute of Physics*. [http://dx.doi.org/10.1063/1.4772207]

Photoluminescence (PL) has been demonstrated to be a versatile technique for nondestructive, noncontact all-optical diagnostics of silicon wafers and solar cells.[1–5] Camera-based imaging, compared to point-by-point laser scan imaging, is a fast method for spatially resolved characterization, thus having excellent industrial application prospects for in-line non-destructive testing (NDT).[6] Steady-state PL imaging critically depends on the accuracy of the applied calibration procedure, and lateral inhomogeneities in the optical properties of a sample have significant influence on imaging results. Furthermore, dc PL cannot monitor the optoelectronic carrier kinetics of surface and near-subsurface regions due to its depth-integrating character through the signal dependence on the dc carrier diffusion length.

A dynamic mid-infrared lifetime mapping technique, based on the analysis of the time dependence of the transient infrared emission induced by the illumination source, was reported recently.[7,8] This technique does not need intensity calibration, however, limitations are associated with reduced spatial resolution due to internal optical reflections and reduced measurement accuracy due to small signal amplitude. Mid-IR HgCdTe (MCT) cameras, which detect thermal electromagnetic radiation in the spectral region above 4 μm, were used in these and prior dynamic measurements.[7–11] However, silicon radiative recombination measurements become complicated due to emission domination by nonradiative (thermal) photons and lattice absorption effects.[12]

Laser-induced infrared photocarrier radiometry (PCR) is a form of dynamic near-infrared modulated PL, spectrally gated to filter out the thermal infrared nonradiative component and retain only the radiative emission spectrum from de-exciting free photocarriers.[12] Frequency-scanned PCR has proven to be an effective non-contact quantitative methodology for the measurement of transport properties in semiconductors.[13–15] In an imaging extension of single-element InGaAs detector PCR, Melnikov *et al.*[16] introduced lock-in carrierography (LIC) as a dynamic near-IR InGaAs camera-based photocarrier radiometric imaging method of solar cells using harmonic laser power modulation. The use of a near-IR camera and optical gating filters totally eliminates thermal IR contributions, thereby enhancing contrast due to localized radiative emission efficiency variations over the surface of a solar cell. Quantitative transport parameter measurements using auxiliary PCR frequency scans were performed,[4] and LIC images have been shown to correspond to microwave photoconductivity-derived lifetime images;[17] however, the combined sequential PCR-LIC process is too slow for in-line inspection purposes using single frequency LIC. Herlufsen *et al.*[18] have implemented a dynamic PL imaging also using an InGaAs camera and lock-in detection based on photocarrier transients. This is a calibration-free method, however, it requires internal calibration between regions of strong and weak PL signals to achieve quantitative PL lifetime measurements.

In this letter LIC is further developed into a quantitative effective lifetime imaging methodology of Si wafers by combining aspects of rapid PCR frequency scanning with camera lock-in imaging. Optical illumination in the experimental imaging system was performed with two fiber coupled 9-W 808-nm infrared diode lasers. The laser beams were spread and homogenized by microlens arrays forming a 10×10 cm^2 square illumination area with intensity variations <5% across that area. A high-speed near-IR InGaAs camera (SU320KTSW-1.7RT/RS170 from Goodrich Sensors Unlimited; 320×256 pixel active elements) was used with spectral bandwidth 0.9–1.7 μm, frame rate 119.6 fps for full window size, and full-frame exposure times ranging from 0.13 ms to 16.6 ms. To acquire high signal-to-noise-ratio lock-in in-phase and quadrature images, a 16$\times$ undersampling lock-in method was applied to the output image frames. The exposure time of the camera was chosen to be 0.52 ms, so the modulation frequency of the laser could reach 400 Hz. A data acquisition module USB 6259 from National Instruments was used to generate a square waveform for laser current modulation, as well as to trigger frame acquisition signals in the camera. The camera images were read by the computer using a PCI-1427 frame grabber from National Instruments to produce computer-generated amplitude and phase images. A schematic of the setup can be found elsewhere.[16,19] All measurements were made at room temperature in the dark.

The sample under investigation was a p-type crystalline silicon wafer with thickness 520 μm. A small area of the backside surface of the wafer was mechanically damaged through gentle rubbing with fine sandpaper. Figure 1 shows the LIC amplitude and phase images obtained at 300 Hz modulation frequency. The overall measurement and data acquisition time was ca. 3 min, corresponding to 100 averages. There is substantial contrast in both amplitude and phase images of Fig. 1 with the damaged area located at the bottom center. The physical origin of the contrast in the carrierographic images is related to variations in modulated photocarrier-wave density.[16] Qualitative comparison between amplitude and phase images shows the expected correspondence: large amplitude is due to high photocarrier density, i.e., long local effective carrier recombination lifetime and thus large phase lag. Owing to the variable reflectance dependence on location across industrial Si wafers which is incorporated in the carrierographic amplitude, but not in the phase, only phase images were considered for quantitative analysis. Furthermore, PCR and carrierographic amplitude depends supralinearly on laser intensity,[20] whereas the lock-in phase has a Fourier coefficient at the fundamental frequency $f = \omega / 2\pi$. The mechanical damage on the back side has led to significant reduction in effective carrier recombination lifetime and an increase in back surface recombination velocity (SRV).

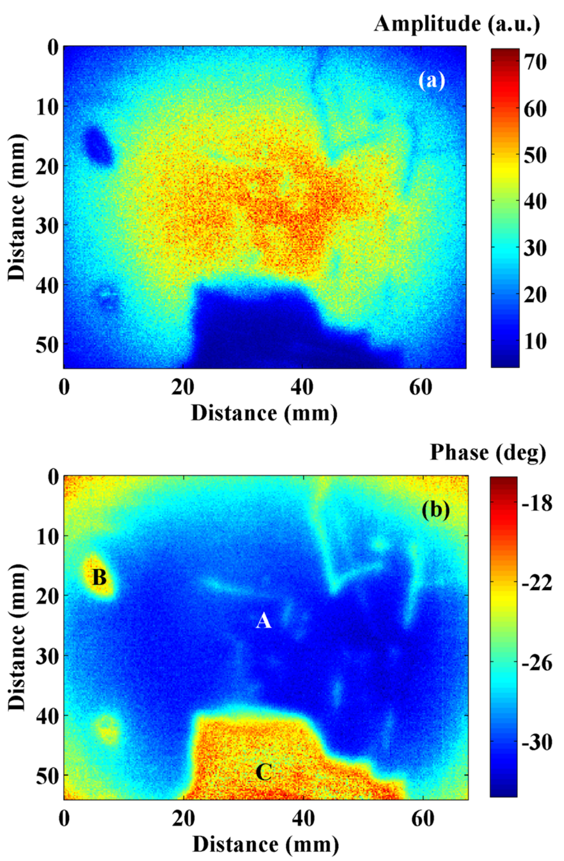

FIG. 1. LIC amplitude and phase images of a Si wafer with mechanical back-side damage. Points A-C were selected for full PCR frequency scans.

Although the optical absorption depth at the excitation wavelength is very short (a few micrometers), the image clearly reveals the damaged area 500 μm deep through the back-surface recombination of the photo-excited free-carrier density wave. The nonradiative recombination centers at the bottom of the images in Fig. 1 generated contrast due to compromised radiative recombination and low free-carrier density. The mechanical damage in that area led to decreasing amplitude (amplitude contrast) with smaller phase lag (phase contrast).

PCR frequency scans are known to yield information about four optoelectronic transport properties of semiconductor materials and devices: bulk recombination lifetime, front and back SRVs, and ambipolar diffusivity.[12] These parameters ultimately control the contrast in lock-in carrierography, depending on the modulation frequency.[16] To ensure proper quantitative functionality of the LIC system, PCR frequency scans with a single-element InGaAs detector Thorlabs model PDA400 with a built-in preamplifier and a noise equivalent power figure of $2.9-8.2 \times 10^{-12}$ W Hz$^{-1/2}$ were also carried out. For comparison of our camera results with the single-element detector, PCR frequency scans were also performed from 10 to 400 Hz. Figure 2 demonstrates the excellent agreement of phase-frequency dependence between the InGaAs camera and single-element detector measurements, which is convincing evidence that quantitatively accurate lifetime images were possible with our camera-based system. Three characteristic locations on the wafer were investigated: Point A at the central intact part and points B and C, located in areas with different degrees of damage.

The linearized lock-in PCR and carrierographic signals from optoelectronic semiconductors, and Si in particular, depend mainly on the free-carrier-wave density integral,[12]

$$S(\omega) = F(\lambda_1, \lambda_2) \int_0^L \Delta N(z, \omega) \mathrm{d}z. \quad (1)$$

This consists of contributions from radiative recombination in the bulk and at the surface, whereas enhanced nonradiative recombination at, and decreased radiative emissions

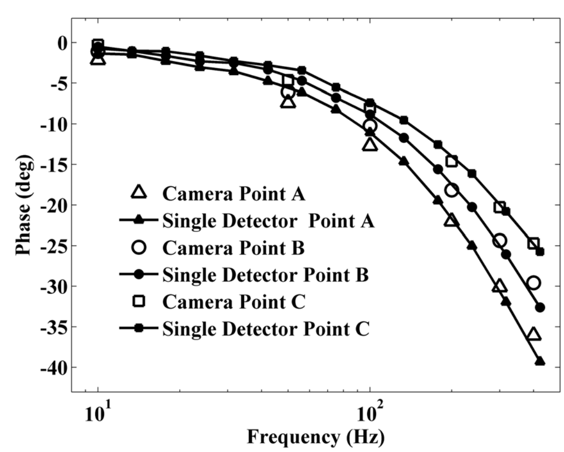

FIG. 2. Comparison of the phase-frequency dependence between camera and single-element InGaAs detector. The modulation frequencies of the camera-based measurement were chosen to be 10 Hz, 50 Hz, 100 Hz, 200 Hz, 300 Hz, and 400 Hz.

from, the damaged back surface create imaging contrast, provided the frequency is low enough for the modulus of the ac carrier diffusion length,

$$L(\omega) = \sqrt{\frac{D^* \tau_b}{1 + i\omega\tau_b}}, \qquad (2)$$

to be larger than, or on the order of, the wafer thickness, L. In Eq. (1), F is a function of the spectral bandwidth (λ_1, λ_2) of the detector; $\Delta N(z,\omega)$ is the optically generated excess free-carrier-wave density at modulation angular frequency ω and at depth z. In Eq. (2), D^* is the ambipolar carrier diffusivity and τ_b is the bulk lifetime.

In principle, the four transport parameters can be obtained through a typical lock-in amplifier 10 Hz–100 kHz phase-frequency dependence.[12] However, due to camera exposure time limitations (exposure time should not be longer than a quarter of the modulation period), the maximum frequency of the camera-based measurements was 400 Hz, too low for the determination of all the transport parameters. Given the primary sensitivity of PCR frequency dependence to bulk recombination lifetime and SRV, and the practical need to speed up the quantitative imaging computational process, the phase-frequency curves in Fig. 2 were best-fitted to a simplified version of the integrated diffuse carrier-wave density $\Delta N(z,\omega)$ model[12] replaced by a rate equation model,[15,16]

$$S(\omega) = \frac{\tau_e K}{1 + i\omega\tau_e}, \qquad (3)$$

where K is a material-property-dependent constant and τ_e is the *effective* lifetime which is a combination of the bulk and surface lifetimes,[21]

$$\tau_e = \left(\frac{1}{\tau_b} + \frac{1}{\tau_s}\right)^{-1}. \qquad (4)$$

Here τ_s is the surface lifetime, a function of the SRVs. The phase of the simplified model has the form,

$$\varphi(\omega) = -\tan^{-1}(\omega\tau_e). \qquad (5)$$

With the phase-frequency dependence of all pixels in the carrierographic image fitted to Eq. (5), the effective carrier lifetime map was obtained and is shown in Fig. 3.

The lifetime map in Fig. 3 shows similar features to the amplitude and phase images of Fig. 1.[3] It should be mentioned, that the central region of the wafer shows the highest lifetime values which decrease closer to the rim, which is typical for crystalline Si wafers. In principle, one can obtain a quantitative lifetime map directly from the phase image at a fixed frequency. However, there may be instrumental phase offset issues which prevent the self-calibration of the technique. Figure 3 is more accurate because it is extracted from six phase images at different frequencies including the $\omega\tau_e > 1$ range which is sensitive to bulk and surface recombination rates.[1] Lifetime measurement *accuracy* was estimated by comparing the camera results with the single-element detector. Lifetime values at Points A-C, extracted from the camera phase-frequency dependencies shown in Fig. 2, are 303 μs, 238 μs, and 192 μs, respectively; those

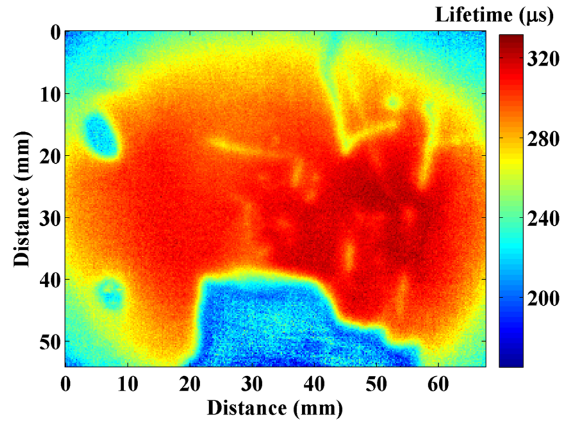

FIG. 3. Lifetime map calculated from the phase-frequency dependence of six carrierographic images.

extracted from the single detector phase-frequency dependencies are 312 μs, 244 μs, and 189 μs, respectively. The relative error is within 3%. Furthermore, lifetime measurement *"precision"* is determined by the size of the standard deviations in the frequency response curve of the image. The absolute phase standard deviation is less than 0.08°, which is indistinguishable from the size of the symbols used as data points in Fig. 2 (the PCR system is very stable in the range from 10 to 400 Hz). Based on these facts, the range of lifetime values measured for each point A-C has uncertainty of 0.14%. This amounts to only 1 μs of the absolute values of the lifetimes calculated for these points. Therefore, the fitting procedure to Eq. (5) can offset measurement errors and yield high LIC self-consistency, self-calibration, and stand-alone reliability.

In conclusion, in this paper LIC has been developed into a quantitative effective lifetime imaging technique, verified through comparing the phase-frequency dependence to conventional PCR single-element InGaAs detector results. Using LIC phase image frequency scans from 10 Hz–400 Hz, effective lifetime maps can be obtained. Although the LIC phase channel yields absolute quantitative lifetime images, for the unique determination of all four transport parameters access to higher frequency images is required. Additional advantages associated with high-frequency imaging at $f \gg (2\pi\tau_e)^{-1}$ are: (a) the short ac diffusion length which is the key to high spatial and axial resolution of LIC images, consistent with Eq. (3); and (b) the ability to resolve the SRVs and the ambipolar diffusivity. Resolving these parameters will enable LIC to reconstruct quantitative images of all four transport properties in Si wafers in a self-calibrated manner.

The authors are grateful to NSERC for a Discovery grant, to the Canada Foundation for Innovation (CFI) for equipment grants, and to the Ontario Ministry for Research and Innovation (MRI) for the Inaugural Premier's Discovery Award in Science and Technology (2007).

[1] I. Riisness, C. Carach, and M. J. Gordon, Appl. Phys. Lett. **100**, 073308 (2012).
[2] A. Delamarre, L. Lombez, and J. F. Guillemoles, Appl. Phys. Lett. **100**, 131108 (2012).
[3] E. Olsen and A. S. Flø, Appl. Phys. Lett. **99**, 011903 (2011).
[4] J. A. Giesecke, M. C. Shubert, B. Michl, F. Schindler, and W. Warta, Sol. Energy Mater. Sol. Cell **95**, 1011 (2011).

[5]T. Trupke, R. A. Bardos, M. C. Schubert, and W. Warta, Appl. Phys. Lett. **89**, 044107 (2006).
[6]I. Latchford and B. True, "Solar inspection: Keeping an eye on quality control," Photovoltaics World, **2011**(4), July/August.
[7]K. Ramspeck, S. Reissenweber, J. Schmidt, K. Bothe, and R. Brendel, Appl. Phys. Lett. **93**, 102104 (2008).
[8]K. Ramspeck, K. Bothe, J. Schmidt, and R. Brendel, J. Appl. Phys. **106**, 114506 (2009).
[9]P. Pohl, J. Schmidt, C. Schmiga, and R. Brendel, J. Appl. Phys. **101**, 073701 (2007).
[10]M. Kasemann, M. C. Schubert, M. The, M. Köber, M. Hermle, and W. Warta, Appl. Phys. Lett. **89**, 224102 (2006).
[11]P. Pohl, J. Schmidt, K. Bothe, and R. Brendel, Appl. Phys. Lett. **87**, 142104 (2005).
[12]A. Mandelis, J. Batista, and D. Shaughnessy, Phys. Rev. B **67**, 205208 (2003).
[13]J. Batista, A. Mandelis, and D. Shaughnessy, Appl. Phys. Lett. **82**, 4077 (2003).
[14]J. Batista, A. Mandelis, D. Shaughnessy, and B. C. Li, Appl. Phys. Lett. **85**, 1713 (2004).
[15]A. Mandelis, A. Melnikov, J. Tolev, J. Xia, S. Huq, and E. Lioudakis, Quant. Infrared Thermography J. **7**, 35 (2010).
[16]A. Melnikov, A. Mandelis, J. Tolev, P. Chen, and S. Huq, J. Appl. Phys. **107**, 114513 (2010).
[17]A. Melnikov, B. Halliop, A. Mandelis, and N. P. Kherani, Thin Solid Films **520**, 5309 (2012).
[18]S. Herlufsen, K. Ramspeck, D. Hinken, A. Schmidt, J. Muller, K. Bothe, J. Schmidt, and R. Brendel, Phys. Stat. Sol. RRL **5**(1), 25 (2011).
[19]A. Mandelis, Y. Zhang, and A. Melnikov, J. Appl. Phys. **112**, 054505 (2012).
[20]J. Tolev, A. Mandelis, and M. Pawlak, J. Electrochem. Soc. **154**, H983 (2007).
[21]D. K. Schroder, IEEE Trans. Electron Dev. **44**, 160 (1997).